

**Frustration-induced itinerant ferromagnetism of fermions in optical lattices**Chengshu Li,<sup>1</sup> Ming-Gen He,<sup>2,3</sup> Chang-Yan Wang,<sup>1</sup> and Hui Zhai<sup>1,\*</sup><sup>1</sup>*Institute for Advanced Study, Tsinghua University, Beijing 100084, China*<sup>2</sup>*Hefei National Research Center for Physical Sciences at the Microscale and School of Physical Sciences, University of Science and Technology of China, Hefei 230026, China*<sup>3</sup>*CAS Center for Excellence in Quantum Information and Quantum Physics, University of Science and Technology of China, Hefei 230026, China*

(Received 22 May 2023; revised 31 March 2024; accepted 2 April 2024; published 16 April 2024)

When the Fermi Hubbard model was first introduced 60 years ago, one of the original motivations was to understand the correlation effects in itinerant ferromagnetism. In the past two decades, ultracold Fermi gas in an optical lattice has been used to study the Fermi Hubbard model. However, the metallic ferromagnetic correlation was observed only in a recent experiment using frustrated lattices, and its underlying mechanism is not yet clear. In this paper, we point out that, under the particle-hole transformation, the single-particle ground state can exhibit double degeneracy in such a frustrated lattice. Therefore, the low-energy state exhibits valley degeneracy, reminiscent of multiorbit physics in ferromagnetic transition metals. The local repulsive interaction leads to the valley Hund's rule, responsible for the observed ferromagnetism. We generalize this mechanism to distorted honeycomb lattices and square lattices with flux. This mechanism was first discussed by Müller-Hartmann in a simpler one-dimensional model. However, this mechanism has not been widely discussed and still needs to be related to experimental observations. Hence, our study not only explains the experimental findings but also enriches our understanding of itinerant ferromagnetism.

DOI: [10.1103/PhysRevB.109.165131](https://doi.org/10.1103/PhysRevB.109.165131)**I. INTRODUCTION**

Itinerant ferromagnetism has been discovered in nature for thousands of years [1]. However, a complete understanding of its microscopic origin is still challenging. The Stoner mean-field theory has predicted itinerant ferromagnetism in metal when the repulsive interaction between fermions exceeds a critical value [2]. When such ferromagnetism occurs, the Pauli exclusion principle increases kinetic energy considerably. Therefore, the critical interaction strength predicted for Stoner ferromagnetism is comparable to the Fermi energy. Under such a strong interaction strength, the correlation effect can no longer be ignored. The competition from other strongly correlated nonmagnetic states usually takes over Stoner ferromagnetism. Therefore, understanding itinerant ferromagnetism becomes essentially a strongly correlated problem.

When the Hubbard model was introduced in the middle of the last century [3–5], one major purpose was to understand the correlation effect in ferromagnetism. Unfortunately, the consensus on ferromagnetism in the Hubbard model is still limited after many decades [6–9]. Rigorous results can only be obtained for exceptional cases such as Nagaoka ferromagnetism [10–12] and flat-band ferromagnetism [13]. Nagaoka ferromagnetism considers a single-hole doping away from half filling in the limit of infinite repulsion, and flat-band ferromagnetism requires fine tuning of particle hopping to reach a flat-band dispersion. Moreover, the single-band

Hubbard model is usually oversimplified to directly compare with experiments on real materials.

Ultracold atoms in optical lattices directly realize the Hubbard model and provide a new opportunity to study the physics therein [14,15]. However, the temperature of atoms in optical lattices cannot be cooled much below the kinetic energy, which prevents observing possible low-temperature orderings, such as fermion pairing, at this stage. In contrast, ferromagnetism often occurs in a relatively high temperature. It is conceivable that one does not need to enter an extremely low-temperature regime in order to study ferromagnetism in optical lattices. Hence, understanding the nature of ferromagnetism is a potential goal for the current quantum simulations with optical lattices.

Nevertheless, although the Fermi Hubbard model has been realized with ultracold atoms in optical lattices for nearly two decades, itinerant ferromagnetism has not been observed in this system until a very recent experiment [16]. In this experiment, a novel experimental technology allows continuously tuning the lattice geometry from a square to a frustrated triangular lattice. Short-range ferromagnetic correlation has been observed in the particle doping regime when the lattice geometry is tuned close to the triangular regime. However, a convincing theoretical understanding of the physical mechanism behind the observed ferromagnetism is still lacking.

**II. REVIEW OF EXPERIMENTAL SETTING**

This experiment reports an actively phase stabilized optical lattice that can continuously tune the lattice geometry from a square lattice to triangular lattice. The tight-binding model

\*hzhai@tsinghua.edu.cn

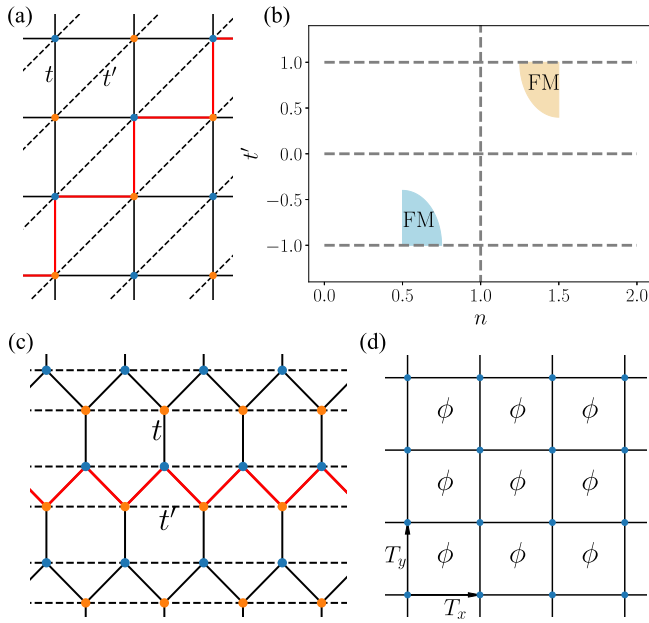


FIG. 1. (a) The tunable optical lattice realized in a recent experiment. (b) The ferromagnetic correlation found in the experiment is marked by the shaded yellow regime in the  $n - t'$  phase diagram, which is mapped to the shaded blue area under the particle-hole transformation. (c) Honeycomb lattice with nearest-neighbor and horizontal next-nearest-neighbor hopping. (d) Square lattice with nearest-neighbor hopping only, but with magnetic flux in each plaquette. The red lines in (a) and (c) denote the one-dimensional chain considered by Müller-Hartmann's paper.

of this lattice is shown in Fig. 1(a). This experiment explores spin-1/2 fermions in such a lattice, and the model is written as

$$\hat{H} = -t \sum_{\langle ij \rangle \sigma} \hat{c}_{i\sigma}^\dagger \hat{c}_{j\sigma} - t' \sum_{\langle\langle ij \rangle\rangle} \hat{c}_{i\sigma}^\dagger \hat{c}_{j\sigma} + U \sum_i \hat{n}_{i\uparrow} \hat{n}_{i\downarrow}, \quad (1)$$

where  $\sigma = \uparrow, \downarrow$  denotes two spin components. The hopping between the nearest neighbor  $\langle ij \rangle$  is denoted by  $t$ , and between the next-nearest neighbor along the dashed line direction  $\langle\langle ij \rangle\rangle$  is denoted by  $t'$ . Both  $t$  and  $t'$  are positive. The next-nearest hopping along another diagonal direction is negligible. When  $t'$  increases from zero to  $t' = t$ , it continuously tunes the lattice geometry from a square lattice to a triangular lattice.  $U$  denotes the interaction strength of on-site repulsion, and  $U/t \approx 9$  in this experiment. In the numerical calculations below, we set  $U$  to be positive infinity in order to explore a larger system size, and the model is reduced to a  $t$ - $J$  model with  $J = 0$ .

This experiment finds ferromagnetic correlation when  $t'/t > 0.5$  and when total fermion density  $n$  exceeds half filling  $n = 1$  and is somewhat close to  $n = 1.5$ . The regime where ferromagnetism is observed is marked by the shaded yellow area in Fig. 1(b). This experiment has only explored the density regime  $0.5 < n < 1.5$  and it is not clear whether the ferromagnetic correlation can also exist when  $n$  exceeds 1.5. The physical origin of this observed ferromagnetism is also not clear yet. Possible scenarios mentioned include the existence of van Hove singularity at  $n = 1.5$  for a triangular

lattice and the possible connection to the Nagaoka ferromagnetism [16–19].

### III. PARTICLE-HOLE TRANSFORMATION

For the benefit of later discussion, we make a particle-hole transformation  $\hat{c}_{i\sigma} \rightarrow (-1)^{i_x+i_y} \hat{c}_{i\sigma}^\dagger$ , where  $i = (i_x, i_y)$  is the site label. If  $t' = 0$ , this transformation keeps the form of Hamiltonian Eq. (1) invariant. The  $t'$  term is what causes frustration in this lattice, and for the same reason, the  $t'$  term is not invariant under the particle-hole transformation. Instead, this transformation changes  $t'$  to  $-t'$ . This corresponds to inserting a  $\pi$  flux in each triangle. For positive  $t'$ , the system essentially describes particles moving in a real potential and all hopping terms have negative matrix elements that satisfy Feynman's no-node theorem [20]. Therefore, the single-particle ground state cannot have degeneracy. However, for negative  $t'$ , the condition for the no-node theorem is no longer satisfied, and the single-particle ground state can have degeneracy. It turns out that this degeneracy is crucial for explaining this observed ferromagnetism, as it will become clear later.

Under this transformation,  $n = n_\uparrow + n_\downarrow$  becomes  $2 - n$ , that is, the particle doping is mapped to hole doping. Thus, the particle-hole transformation maps  $(t', n)$  to  $(-t', 2 - n)$  in the phase diagram shown in Fig. 1(b). Therefore, we can focus solely on the density regime  $0 < n \leq 1$  but include both positive and negative  $t'$ . With this mapping, the regime where ferromagnetism is observed is mapped to the low-density regime with  $t' < -0.5$ , as marked as the shaded blue area in Fig. 1(b).

### IV. NUMERICAL RESULTS

We first present our numerical results in Fig. 2 [21]. All the calculations below are done for infinite positive  $U$ , with the Hamiltonian

$$\hat{H} = -t \sum_{\langle ij \rangle \sigma} \hat{c}_{i\sigma}^\dagger \hat{c}_{j\sigma} - t' \sum_{\langle\langle ij \rangle\rangle} \hat{c}_{i\sigma}^\dagger \hat{c}_{j\sigma} + U \sum_i \hat{n}_{i\uparrow} \hat{n}_{i\downarrow}, \quad U = \infty, \quad (2)$$

and the infinite  $U$  is incorporated in the restricted on-site Hilbert space with no double occupancy. The first calculation is exact diagonalization for two particles with different system sizes, reminiscent of different densities. This calculation can cover the low-density regime up to  $n = 0.5$ . Due to the  $SU(2)$  spin rotational symmetry, the total spin is a good quantum number and all quantum states with the same total spin are degenerate. We find a level crossing between spin singlet and spin triplet states, as shown in Fig. 2(a). The spin triplet states have a lower energy when  $t' < t'_c$ , and the value of  $t'_c$  approaches  $-0.5$  when the system size is large enough.

The second calculation is the density-matrix renormalization group (DMRG) calculation with a finite number of fermions on a different strip geometry. We can calculate  $\langle \hat{S}_{\text{tot}}^2 \rangle$  with  $\hat{S}_{\text{tot}} = \sum_i \hat{S}_i$  for the ground state, and  $S_{\text{tot}}$  is given by  $\langle \hat{S}_{\text{tot}}^2 \rangle = S_{\text{tot}}(S_{\text{tot}} + 1)$ . In the calculations we fix  $S_{\text{tot}}^z = 0$ , in which sector one expects the  $S_{\text{tot}} = N/2$  and  $S_{\text{tot}} = 0$  to have a similar level of entanglement, a key to guaranteeing that the DMRG routine is unbiased and amenable to a reasonable bond dimension. We find a transition from  $S_{\text{tot}} = N/2$  to  $S_{\text{tot}} = 0$

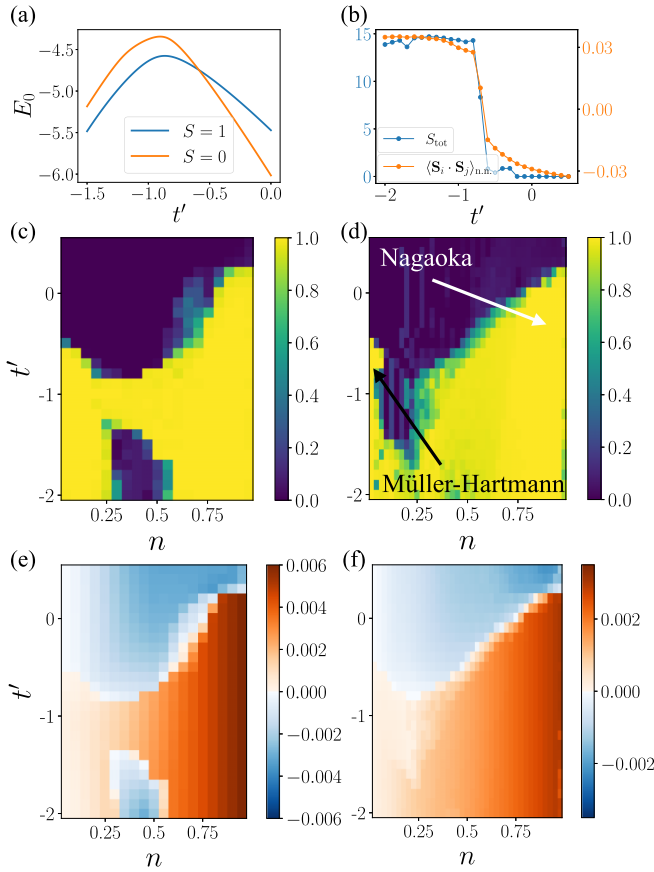


FIG. 2. (a) Two-body problem in a  $4 \times 4$  lattice with an open boundary condition. The singlet and triplet state energies as a function of  $t'$ . (b) The total spin  $S_{\text{tot}}$  and nearest-neighbor correlation function  $\langle \mathbf{S} \cdot \mathbf{S} \rangle_{n,n}$  of the ground state calculated by the DMRG method for  $N = 30$  particles in a  $4 \times 20$  strip. Here,  $S_{\text{tot,max}} = N/2 = 15$ . (c), (d) The total spin  $S_{\text{tot}}$  as a function of  $n$  and  $t'$ , normalized by the maximum total spin of the filling  $S_{\text{tot,max}} = N/2$ , for (c)  $2 \times 20$  and (d)  $4 \times 20$  strips, respectively. (e), (f) The nearest-neighbor correlation function  $\langle \mathbf{S} \cdot \mathbf{S} \rangle_{n,n}$  as a function of  $n$  and  $t'$ , normalized by the particle number  $N$ , for  $2 \times 20$  and  $4 \times 20$  strips, respectively. All DMRG calculations have bond dimension  $\chi = 1400$ .

around  $t' = t'_c$ , as shown in Fig. 2(b). We also calculate the nearest-neighbor correlation function  $\langle \mathbf{S} \cdot \mathbf{S} \rangle_{n,n}$ , averaged over all bonds of the square lattice. We find clear evidence of ferromagnetic to antiferromagnetic correlations, as shown in Fig. 2(b). The same calculation is carried out for a wide range of  $n$  and  $t'$ , and the results are collected in Figs. 2(c)–2(f). Here, for better comparison and visualization the results are normalized by  $S_{\text{tot,max}} = N/2$  and  $N$  for Figs. 2(c) and 2(d) and Figs. 2(e) and 2(f), respectively.

A notable feature in Figs. 2(c)–2(f) is that for all calculations,  $t'_c$  approaches  $-0.5$  at the low-density limit when  $n \rightarrow 0$ . Below we will explain why  $t' = -0.5$  is a special point, and the ferromagnetism emerged in this regime will be called the *Müller-Hartmann mechanism*. In this regime, the general trend is that  $t'_c$  decreases as  $n$  increases.

Nearby half filling with  $n = 1$ , it is known that hole doping can result in Nagaoka ferromagnetism at infinite  $U$ . Strictly speaking, Nagaoka ferromagnetism can only be proved for

single-hole doping with  $t' < 0$ . However, our numerical results show that when  $t' = 0$ , the Nagaoka ferromagnetism can exist up to  $\sim 20\%$  of hole doping, that is, for  $0.8 \lesssim n < 1$ . This is consistent with previous numerical results [22]. Hence, we attribute the ferromagnetism nearby half filling as the *Nagaoka mechanism*. In this regime,  $t'_c$  also decreases when  $n$  decreases from  $n = 1$ , and this density dependence of  $t'_c$  is opposite to that found in the low-density regime.

Hence, we have identified two different mechanisms of ferromagnetism from our numerical results, and they emerge from the low-density limit and nearby half filling, respectively. They are characterized by different density dependences of  $t'_c$ . The trend of the experimental observed ferromagnetic boundary, upon the particle-hole transformation, is consistent with the Müller-Hartmann mechanism.

We also note that the phase boundary calculated with  $2 \times 20$  and  $4 \times 20$  converge for low-density and high-density nearby half filling. However, the phase boundary at the intermediate density is still subject to a finite-size effect. Moreover, the physics in the intermediate density connecting these two different mechanisms also requires further investigations.

## V. MÜLLER-HARTMANN MECHANISM

To see why  $t' = -0.5$  is special, we first look at the single-particle dispersion which reads

$$\begin{aligned} \mathcal{E}(k_x, k_y) &= -2t \cos(k_x) - 2t \cos(k_y) - 2t' \cos(k_x + k_y) \\ &= -4t \cos(k_+) \cos(k_-) - 2t' \cos(2k_+), \end{aligned} \quad (3)$$

where  $k_{\pm} = (k_x \pm k_y)/2$ . It is easy to see that the dispersion minimum occurs at  $k_- = 0$ . As shown in Fig. 3(a), when  $t'/t > -0.5$ , the band dispersion has a unique minimum at  $k_+ = 0$ . However, when  $t'/t < -0.5$ , the band dispersion displays two degenerate minima along  $k_+$  axes. That is to say, a Lifshitz transition occurs when  $t'/t = -0.5$ .

The paper by Müller-Hartmann first pointed out that ferromagnetism can occur in the low-density regime when the band minima display double degeneracy [23], followed by a few related works in later literature [24]. This paper considered a one-dimensional chain with next-nearest hopping, and the Hamiltonian reads

$$\hat{H} = - \sum_{i\sigma} (t \hat{c}_{i,\sigma}^\dagger \hat{c}_{i+1,\sigma} + t' \hat{c}_{i,\sigma}^\dagger \hat{c}_{i+2,\sigma} + \text{H.c.}) + U \sum_i \hat{n}_{i\uparrow} \hat{n}_{i\downarrow}. \quad (4)$$

In this model, the band minima also displays double degeneracy when  $t'/t < -1/4$ , where Müller-Hartmann argued that ferromagnetism can occur in the low-density regime. We note that this one-dimensional chain can be naturally embedded into the two-dimensional lattice we considered, as shown in Fig. 1(a). In other word, the two-dimensional lattice realized in this cold atom experiment can be viewed as a two-dimensional generalization of Müller-Hartmann's work.

The physical mechanism behind this ferromagnetism can be called the *valley Hund's rule* [25]. Considering the two-particle case, they can be respectively placed in each minimum of single-particle dispersion. For spin-triplet states, the spatial wave function is antisymmetrized, and the interaction energy automatically vanishes. However, for the spin-singlet

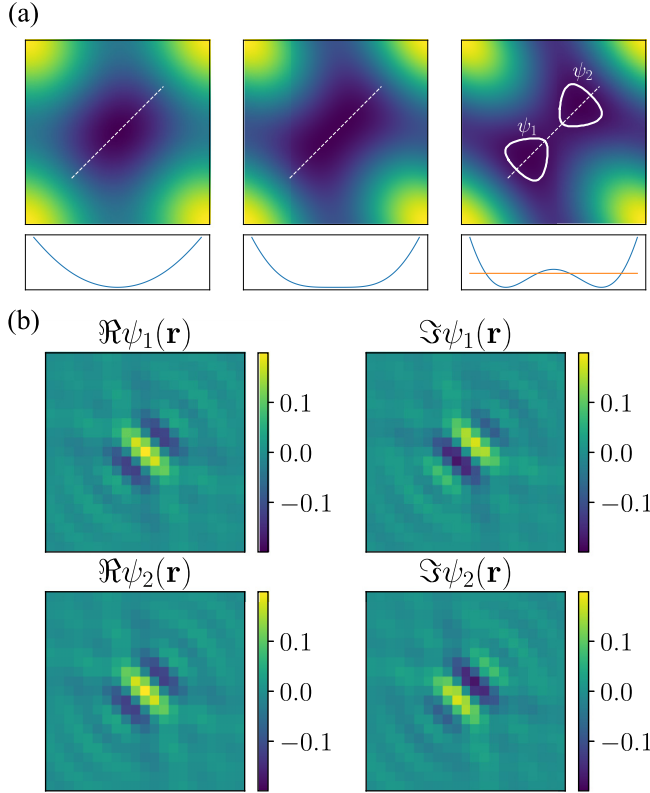


FIG. 3. (a) Single-particle dispersion  $\mathcal{E}(k_x, k_y)$  of the Hamiltonian Eq. (1) for three different values of  $t'$ .  $t' = -0.2$  (left),  $-0.5$  (middle), and  $-0.8$  (right). (b) The real and imaginary parts of two valley Wannier wave functions. These two wave functions are constructed by using the Bloch wave functions around each minimum of single-particle dispersion, as indicated by the solid circle in the right dispersion in (a).

state, one has to apply extra projection to prevent double occupation, which inevitably increases the kinetic energy.

Using the low-energy Bloch wave functions around each minimum, we can construct the effective valley Wannier wave functions for each valley, as shown in Fig. 3(b). These valley Wannier wave functions extend over several lattice sites. The on-site repulsion between fermions effectively introduces Hund's rule between these valley Wannier wave functions. In real materials, itinerant ferromagnetism usually occurs in transition metals with a partially filled  $d$  orbit, and Hund's rule coupling between these  $d$  orbitals is crucial for ferromagnetism. That is to say, the multi-orbital physics plays an essential role. Müller-Hartmann's mechanism says that even for a single-band model, when the single-particle ground state has degeneracy, the valley degeneracy can lead to an emergent multi-orbital physics, resulting in itinerant ferromagnetism at the low-density regime. Since Hund's rule is a local ferromagnetic coupling, we expect that the short-range ferromagnetic correlation caused by this mechanism is robust at finite temperatures. Moreover, since the Hund's rule coupling is the leading-order effect of local repulsion while the antiferromagnetic superexchange interaction is a second-order effect of local repulsion, we also expect that this ferromagnetism is stable with finite interaction strength.

Before concluding this section we discuss how our results at  $T = 0$  relates to the experimentally relevant  $T > 0$  scenario. Throughout the work we focus on  $T = 0$  and the long-range ferromagnetism we find will vanish when  $T > 0$  due to the Mermin-Wagner theorem. On the other hand, the separate calculation of short-range correlation, despite being conducted at  $T = 0$ , is of a more local spirit. In general, such expectation values of local, symmetry-invariant operators tend to be less vulnerable to finite  $T$  than long-range operators or symmetry-covariant operators including the order parameter. Hence, while caution needs to be exercised when directly applying  $T = 0$  results to  $T > 0$ , we expect our  $T = 0$  results to provide useful insights for the experimentally relevant finite  $T$  physics.

## VI. GENERALIZATION TO HONEYCOMB LATTICE

To further confirm our understanding of emergent ferromagnetism in this experiment, we generalize this idea to other models, where degenerate ground states can also be found. The first generalization is fermions in a distorted honeycomb lattice. Similar to the square-lattice model, the nearest-neighbor hopping is denoted by  $t$ . We compress the lattice along the horizontal direction such that we should also include the next-nearest hopping  $t'$  along the horizontal dashed line direction, as shown Fig. 1(c). This lattice can also be viewed as a set of  $t - t'$  chains along the  $\hat{x}$  direction considered by Müller-Hartmann's paper, coupled vertically along the  $\hat{y}$  direction. We introduce a similar particle-hole transformation that only changes the sign of  $t'$ . The ground state of this dispersion also shows a Lifshitz transformation from single to double degeneracy at  $t' = -0.25$ , as shown in Fig. 4(b). The phase diagram obtained by DMRG calculation is shown in Fig. 4(a). This phase diagram contains two ferromagnetic regimes, one in the low-density regime around  $t' = -0.25$  and the other nearby half filling for  $t' < 0$ . Clearly, they respectively manifest Müller-Hartmann and Nagaoka mechanisms [26]. Unlike the square-lattice case, these two ferromagnetism mechanisms occur in two disconnected regimes in the phase diagram, clearly visualizing their difference.

## VII. GENERALIZATION TO FLUX LATTICE

The second generalization is a square lattice with a magnetic flux in each plaquette. Here, we only consider the nearest hopping in a square lattice, and the magnetic flux only introduces a phase in the hopping and does not cause Zeeman splitting. However, with magnetic flux  $\phi = 2\pi/m$  in each plaquette ( $m$  is an integer), the translation of one lattice spacing along the  $\hat{x}$  direction does not commute with one lattice space translation along the  $\hat{y}$  direction, and only commutes with the translation of the  $m$  lattice spacing along the  $\hat{y}$  direction. This enlarges the unit cell and leads to  $m$ -fold degeneracy of the dispersion spectrum, as shown in Fig. 5(b). For a fixed magnetic flux, the only tunable parameter is density. In Fig. 5(a), we show the total magnetization as a function of fermion density. It is interesting to note that when  $m = 1$ , the single-particle dispersion is not degenerate but the hopping satisfies the condition for Nagaoka ferromagnetism. Hence, DMRG finds ferromagnetism nearby half filling. In contrast,

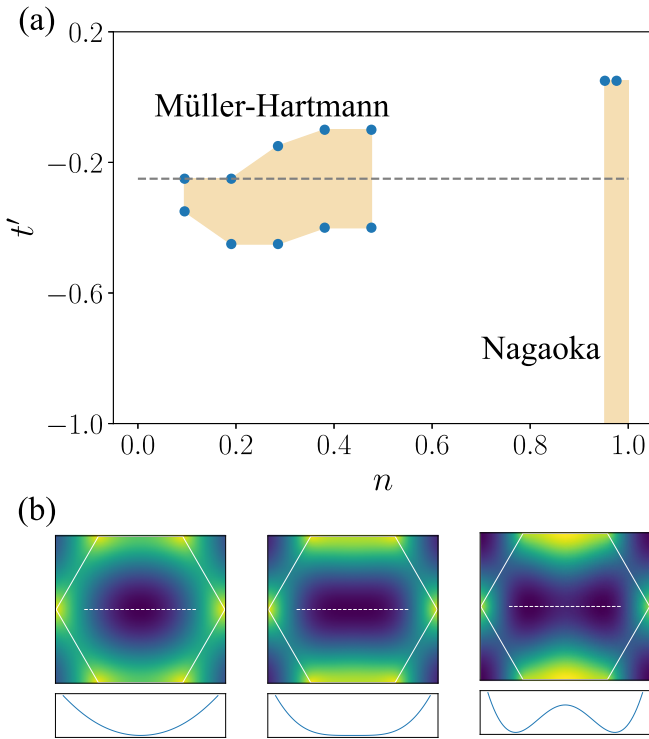


FIG. 4. (a) The ferromagnetic regime indicated by DMRG calculation in the  $n - t'$  phase diagram of the distorted honeycomb lattice. The model is shown in Fig. 1(c), in which  $t'$  denotes the next-nearest hopping along the horizontal dashed line. The DMRG calculation is performed in a  $3 \times 6$  zigzag cylinder, with bond dimension  $\chi = 1400$ . The dashed line indicates the value of  $t'$  for the Lifshitz transition. (b) The single-particle dispersion of the distorted honeycomb lattice, with  $t' = -0.1$  (left),  $= -0.25$  (middle), and  $= -0.4$  (right).

when  $m > 1$ , hopping terms no longer satisfy the condition for Nagaoka ferromagnetism, but the ground-state degeneracy appears. We find a critical  $n_c$  and the system is ferromagnetism when  $n < n_c$ . We find that  $n_c$  is approximately given by  $1/m$ , which corresponds to a half-filled lowest band. Therefore, ferromagnetism occurs in the low-density regime. This clearly

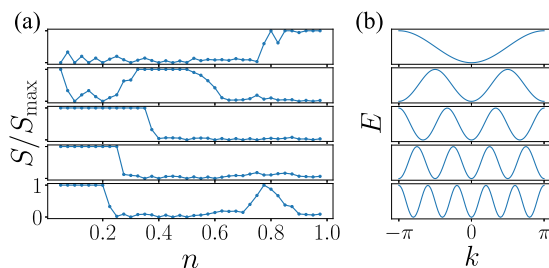


FIG. 5. (a)  $S_{\text{tot}}$  obtained by DMRG calculation.  $S_{\text{max}} = N/2$ . Here, we consider a square lattice with nearest hopping only, but with magnetic flux  $\phi$ .  $\phi = 0, \pi, 2\pi/3, \pi/2$ , and  $2\pi/5$  from the top to the bottom. The DMRG calculation is performed in a  $4 \times 10$  strip with bond dimension  $\chi = 1400$ . (b) The single-particle dispersion around the bottom of the band for different magnetic flux corresponding to (a).

shows Nagaoka and Müller-Hartmann are two different mechanisms.

When taking a closer look at the data in Fig. 5(a), we see that, for the  $\phi = \pi$  case, the nonmagnetic state at  $n \sim 0.1 - 0.3$  is anomalous. We find the results in this density range with  $\phi = \pi$  are quite sensitive to system geometry (e.g., which boundary conditions to choose), and the finite-size effect is quite significant in this density range. There is also a ferromagnetic region around  $n \sim 0.8$  for  $m = 5$  that is beyond simple understanding. These anomalous behaviors again highlight how delicate itinerant ferromagnetism tends to be. Nevertheless, apart from these two anomalies, the general trend as well as the phase transition boundaries at  $1/m$  agree well with our expectations.

## VIII. CONCLUSION AND DISCUSSIONS

In summary, we analyze a recent experiment that first discovers itinerant ferromagnetism in an ultracold atom realization of the Fermi Hubbard model. We attribute the mechanism of this ferromagnetism to the appearance of single-particle ground-state degeneracy. At low density, the valley degeneracy is reminiscent of multiorbital physics in transition metals, and the local repulsive interaction can lead to a valley Hund's rule, resulting in ferromagnetic correlations. This mechanism was first discussed by Müller-Hartmann in a simpler one-dimensional model. Recently, tunable lattice geometry and itinerant ferromagnetism has also been observed in a controlled moiré material [27] and our results might also be relevant for these studies.

We remark that by talking about ferromagnetism, we implicitly assume that the Hamiltonian of the system should not break time-reversal symmetry. In the presence of time-reversal symmetry, the single-particle ground state should not degenerate for a normal kinetic energy term due to Feynman's no-node theorem. In order for the Müller-Hartmann mechanism to apply, the key is frustration plus particle-hole transformation. Because of the lattice frustration, we can effectively inset flux to the hopping terms after a particle-hole transformation, such that the condition for Feynman's theorem is violated. That is why frustration plays an essential role here. Previously, frustration has been considered an essential ingredient for the emergence of exotic phases such as spin liquids [28]; the discussion here shows that frustration can also be a key ingredient responsible for the emergence of ferromagnetism.

## ACKNOWLEDGMENTS

We thank H. Yao, Y. Gu, M. Xu, and P. Pieri for helpful discussions. This work is supported by Innovation Program for Quantum Science and Technology 2021ZD0302005, the Beijing Outstanding Young Scholar Program, the XPLORER Prize, and China Postdoctoral Science Foundation (Grant No. 2022M711868). C.L. is supported by the Chinese International Postdoctoral Exchange Fellowship Program and Shuimu Tsinghua Scholar Program at Tsinghua University. The DMRG calculations are performed using the ITENSOR library (v0.3) [29].

- [1] É. du Trémolet de Lacheisserie, D. Gignoux, and M. Schlenker, *Magnetism: Fundamentals, Materials and Applications* (Springer, New York, 2002), Chap. 1.
- [2] E. C. Stoner, Collective electron ferromagnetism, *Proc. R. Soc. London, Ser. A* **165**, 372 (1938).
- [3] J. Hubbard, Electron correlations in narrow energy bands, *Proc. R. Soc. London, Ser. A* **276**, 238 (1963).
- [4] M. C. Gutzwiller, Effect of correlation on the ferromagnetism of transition metals, *Phys. Rev. Lett.* **10**, 159 (1963).
- [5] J. Kanamori, Electron correlation and ferromagnetism of transition metals, *Prog. Theor. Phys.* **30**, 275 (1963).
- [6] H. Tasaki, The Hubbard model - an introduction and selected rigorous results, *J. Phys.: Condens. Matter* **10**, 4353 (1998).
- [7] H. Tasaki, From Nagaoka's ferromagnetism to flat-band ferromagnetism and beyond: An introduction to ferromagnetism in the Hubbard model, *Prog. Theor. Phys.* **99**, 489 (1998).
- [8] D. P. Arovas, E. Berg, S. A. Kivelson, and S. Raghu, The Hubbard model, *Annu. Rev. Condens. Matter Phys.* **13**, 239 (2022).
- [9] M. Qin, T. Schäfer, S. Andergassen, P. Corboz, and E. Gull, The Hubbard model: A computational perspective, *Annu. Rev. Condens. Matter Phys.* **13**, 275 (2022).
- [10] D. J. Thouless, Exchange in solid  $^3\text{He}$  and the Heisenberg Hamiltonian, *Proc. Phys. Soc.* **86**, 893 (1965).
- [11] Y. Nagaoka, Ferromagnetism in a narrow, almost half-filled  $s$  band, *Phys. Rev.* **147**, 392 (1966).
- [12] H. Tasaki, Extension of Nagaoka's theorem on the large- $U$  Hubbard model, *Phys. Rev. B* **40**, 9192 (1989).
- [13] A. Mielke, Ferromagnetism in the Hubbard model on line graphs and further considerations, *J. Phys. A: Math. Gen.* **24**, 3311 (1991).
- [14] I. Bloch, Ultracold quantum gases in optical lattices, *Nat. Phys.* **1**, 23 (2005).
- [15] I. Bloch, J. Dalibard, and W. Zwerger, Many-body physics with ultracold gases, *Rev. Mod. Phys.* **80**, 885 (2008).
- [16] M. Xu, L. H. Kendrick, A. Kale, Y. Gang, G. Ji, R. T. Scalettar, M. Lebrat, and M. Greiner, Frustration- and doping-induced magnetism in a Fermi-Hubbard simulator, *Nature (London)* **620**, 971 (2023).
- [17] J. Merino, B. J. Powell, and Ross H. McKenzie, Ferromagnetism, paramagnetism, and a Curie-Weiss metal in an electron-doped Hubbard model on a triangular lattice, *Phys. Rev. B* **73**, 235107 (2006).
- [18] I. Morera, M. Kanász-Nagy, T. Smolenski, L. Ciorciaro, A. Imamoğlu, and E. Demler, High-temperature kinetic magnetism in triangular lattices, *Phys. Rev. Res.* **5**, L022048 (2023).
- [19] K. Lee, P. Sharma, O. Vafek, and H. J. Changlani, Triangular lattice Hubbard model physics at intermediate temperatures, *Phys. Rev. B* **107**, 235105 (2023).
- [20] R. P. Feynman, *Statistical Mechanics: A Set of Lectures* (CRC Press, Boca Raton, FL, 1998), Chap. 11.
- [21] The code for our numerical calculations is available at <https://github.com/chengshul/itinerantFM>.
- [22] L. Liu, H. Yao, E. Berg, S. R. White, and S. A. Kivelson, Phases of the infinite  $U$  Hubbard model on square lattices, *Phys. Rev. Lett.* **108**, 126406 (2012).
- [23] E. Müller-Hartmann, Ferromagnetism in Hubbard models: Low density route, *J. Low Temp. Phys.* **99**, 349 (1995).
- [24] P. Pieri, S. Daul, D. Baeriswyl, M. Dzierzawa, and P. Fazekas, Low-density ferromagnetism in the Hubbard model, *Phys. Rev. B* **54**, 9250 (1996).
- [25] Here, "valley" means two sets of low-energy states nearby degenerate single-particle minima, which is different from valley ferromagnetism discussed in the literature, such as N. J. Zhang, J.-X. Lin, D. V. Chichinadze, Y. Wang, K. Watanabe, T. Taniguchi, L. Fu, and J. I. A. Li, Angle-resolved transport non-reciprocity and spontaneous symmetry breaking in twisted trilayer graphene, *Nat. Mater.* **23**, 356 (2024).
- [26] E. Bobrow, K. Stubis, and Y. Li, Exact results on itinerant ferromagnetism and the 15-puzzle problem, *Phys. Rev. B* **98**, 180101(R) (2018).
- [27] E. Anderson, F.-R. Fan, J. Cai, W. Holtzmann, T. Taniguchi, K. Watanabe, D. Xiao, W. Yao, and X. Xu, Programming correlated magnetic states via gate controlled moiré geometry, *Science* **381**, 325 (2023).
- [28] L. Balents, Spin liquids in frustrated magnets, *Nature (London)* **464**, 199 (2010).
- [29] M. Fishman, S. R. White, and E. M. Stoudenmire, The ITensor software library for tensor network calculations, *SciPost Phys. Codebases* **4** (2022).